Research Article

A Late Holocene climate reconstruction from the high-altitude Lake Gölcük sedimentary records, Isparta (SW Anatolia)

Iliya Bauchi Danladi[a,b]* (ID), Sena Akçer-Ön[a], Thomas Litt[b], Z. Bora Ön[a] and Lukas Wacker[c]

[a]Department of Geological Engineering, Faculty of Engineering, Muğla Sıtkı Koçman University, 48000, Kötekli, Muğla, Turkey; [b]University of Bonn, Steinmann Institute of Geology, Mineralogy and Paleontology, Nussallee 8, 53115, Bonn, Germany and [c]Laboratory of Ion Beam Physics, Department of Physics, ETH Zürich, Zürich, CH 8093, Switzerland

Abstract

A high-resolution multiproxy lake sediment dataset, comprising lithology, radiography, µXRF elemental, magnetic susceptibility (MS), δ^{13}C, and δ^{18}O measurements since ca. AD 400 is presented in this study. Changes in lithology, radiography, magnetic susceptibility (MS), δ^{13}C, and δ^{18}O reflect wet/dry climate periods, whereas variability in log(Ca/K) can reflect warm/cold climate periods. Analyses of the multiproxy results allow the distinction of several climate periods, which may be associated with climatic phenomena such as changes in North Atlantic Oscillation (NAO) and/or solar activity. The influence of NAO−/NAO+ (negative/positive) is suggested to be related with the southward/ northward displacement of the storm tracks resulting from the NAO−/NAO+ phases. For solar activity, the influence is explained through a direct increase in solar heating leading to calcite precipitation. The Dark Ages Cold Period (DACP, AD 450–750) reflects cold-dry climate conditions at this site, indicative of a positive North Atlantic Oscillation (NAO+) and low solar activity. The Medieval Climate Anomaly (MCA, AD 950–1250) exhibits wet-dry-wet and warm-cold-warm climate conditions. The wet/dry periods likely are associated with NAO −/NAO+, respectively, and the warm/cold period may reflect relatively high/low solar activity. The Little Ice Age (LIA, AD 1400–1850) is characterized by dry and cold climate conditions, suggesting the influence of NAO+ and low solar activity. Comparison of the results of this study with local and regional results suggests a generally similar climate pattern, which is indicative of similar climate mechanisms. The contradictions can be associated with age-related uncertainties, orographic differences, and/or other regional teleconnections.

Keywords: Lacustrine environment, Paleoclimate, Dark Ages Cold Period, Medieval Climate Anomaly, Little Ice Age, NAO, Solar activity

(Received 28 July 2022; accepted 11 May 2023)

INTRODUCTION

High-altitude lakes, which are located in remote regions of the globe with absence of human settlements and anthropogenic disturbances, are valuable environments that allow continuous sediment accumulation over a long period of time. Therefore, sediments that are deposited in such environments are important for paleoclimate reconstruction and identification of climate cycles/periods (Engstrom and Wright, 1984; Li and Ku, 1997; Cohen, 2003; Martin-Puertas et al., 2017; Żarczyński et al., 2019).

The Holocene is an important geologic epoch encompassing both shortened and extended alternations of climate periods (Turner, 1997; Kuhlmann et al., 2004; Maxbauer et al., 2019). As a result, the Holocene is important for understanding paleoclimate variability as well as current and future climate changes, which are anticipated to be dominated by human-induced changes (Cook et al., 2016; Han et al., 2019). Within the Holocene epoch, the Late Holocene is of particular importance in terms of understanding paleoclimate and current climate changes (Corella et al., 2013; Viana et al., 2014). A large number of European Late Holocene reconstructed paleoclimate studies have reported a drier/colder Dark Ages Cold Period (DACP, ca. AD 400–750), wetter/warmer climate events (Medieval Climate Anomaly, MCA, ca. AD 950–1250), and a drier/colder period (Little Ice Age, LIA, ca. AD 1400–1850) (Baker et al., 2015; Koutsodendris et al., 2017; Moreno et al., 2019). The DACP has been reported as a cold period with societal impacts (Helama et al., 2017). Reports from historical sources suggest there were crop failures, famine, flood, and turmoil during the MCA and LIA (Brázdil et al., 2018). Although, synchronicity issues between geographical locations and/or atmospheric circulation remain unresolved, the DACP, MCA and LIA have been widely used in the literature between ca. AD 400–750, ca. AD 950–1250, and ca. AD 1400–1850, respectively (Mann et al., 2009; Sachs et al., 2009). Global atmospheric circulation patterns, volcanic forcing and solar activity were proposed as possible reasons for the underlying climate events (Goosse et al., 2006; Cronin et al., 2010; Pyrina et al., 2019).

The eastern Mediterranean (EM) is an area of significant historical and archaeological importance, and the seasonal precipitation patterns are vital for the ecosystem and inhabitants of the region (Roberts et al., 2012). Moreover, the region is susceptible to extreme weather events such as flash floods and heat waves, which can have severe effects on the local population and environment. Similar to under-reported regions in which few studies

exist, the spatio-temporal character of the DACP, MCA, and LIA are still unresolved. Although previous research has linked them to changes in climate modes (e.g., North Atlantic Oscillation, NAO), orographic differences, volcanic activities, prolonged sea ice/oceanic feedbacks, and solar activity, more regional studies are needed (Goosse et al., 2006; Roberts et al., 2012; Kushnir and Stein, 2019). Links of the DACP, MCA, and LIA to socio-political developments in the EM have also been investigated (Bar-Matthews et al., 1998; Xoplaki et al., 2016). In line with most published records in the North Atlantic region (Mann, 2013; Auger et al., 2019), the EM records reveal a wet MCA and dry LIA associated with alternating pattern of NAO (Roberts et al., 2012; Lüning et al., 2019). Although, NAO is an important component of climate variability in the region, interplay of other factors such as Mediterranean Sea surface temperature, orographic differences, North Sea/Caspian Pattern (NCP), Atlantic Multidecadal Oscillation, and East-Atlantic Pattern could not be ruled out (Bozkurt and Sen, 2011; Roberts et al., 2012; Lüning et al., 2019). Therefore, the mechanisms behind the unprecedented climate changes are still a subject of discussion.

In accordance with the EM studies, an emerging body of literature on Anatolia is focused on understanding climate changes during the MCA and LIA (Cullen and deMenocal, 2000; Akkemik and Aras, 2005; Touchan et al., 2007; Kuzucuoğlu et al., 2011; Woodbridge and Roberts, 2011; Heinrich et al., 2013; Tudryn et al., 2013; Ocakoğlu et al., 2016; Akçer Ön, 2017; Köse et al., 2017; Danladi and Akçer-Ön, 2018; Kılıç et al., 2018; Erginal et al., 2019). These studies have made significant progress in understanding and linking the climate events with natural modes of climate variability (NAO, East-Atlantic Patterns, NCP, and the Indian Monsoon), orographic differences, volcanic activities, and solar activity. Jones et al. (2006), using a record from annually dated Lake Nar, reported a wet period (AD 1000–1350) and dry LIA (AD 1400–1950), which are related with NAO, NCP, and the Indian Monsoon. Historical literature has documented a wide range of dry conditions during the LIA (White, 2012, 2013; Köse, 2018), which have been confirmed by tree ring reconstructions (Touchan et al., 2007; Köse et al., 2017). However, in Anatolia, high-resolution climate records with robust chronologies are still needed.

In this paper, a high-resolution multi-proxy data investigation of a piston core from Lake Gölcük sedimentary record, combining lithological description, magnetic susceptibility, µXRF elemental analysis, pollen, and stable isotopic measurements of carbon ($\delta^{13}C$) and oxygen ($\delta^{18}O$) is presented. The age-depth model was constructed based on seven radiocarbon dates. The study allows comparison of different climate indicators of the sediment core, which form the basis for a paleoclimate interpretation since AD 400 (1550 cal years BP). To understand the climate variability since AD 400, Lake Gölcük proxies have been compared with NAO reconstruction and solar activity proxy. The records also were compared with regional data to assess the spatio-temporal character of the DACP, MCA, and LIA climate events.

STUDY AREA

Lake Gölcük is a small volcanic crater lake that is located at a high altitude (1380 m asl) in the Isparta Province of SW Anatolia (Fig. 1). Lake Gölcük has a surface area of 1.05 km^2 and a diameter of 1500 m; the deepest measured depth of the lake is 40 m (DSİ, 1978). The lake is located in the Lake District of Isparta

Province in southwestern Anatolia. The region surrounding Gölcük Lake is characterized by volcanic activity, with various volcanic cones and domes in the area. The region has been the subject of extensive research, primarily focused on Quaternary volcanic events, surrounding faults, and lineaments (Cengiz et al., 2006; Platevoet et al., 2008; Schmitt et al., 2014; Canpolat, 2015). The underlying geology is volcanic with andesite and trachyandesites ranging from the Tertiary to the Quaternary (Figure 1).

In terms of vegetation, the lake is situated in the Oro Mediterranean vegetation zone, which presently includes *Quercus cerris*, *Quercus calliprinos*, *Pinus brutia*, and *Pinus nigra* in regions at ~1000 m asl, and *Cedrus libani*, *Abies cilicica*, and *Juniperus* in regions between 1000–2000 m asl (Zeist et al., 1975).

The region is in a boundary close to the continental Anatolian and Mediterranean climate (Deniz et al., 2011). Instrumental records of the Isparta Province documented between 1929 and 2019 show an average annual temperature and precipitation of 12.2°C and 570.2 mm, respectively (Danladi et al., 2021). High pressure systems over Europe, North Africa, and monsoon regions combined with the Mediterranean SST influence the temperature and precipitation variations in the region (Bozkurt and Sen, 2011).

METHODOLOGY

A 198-cm-long continuous, undisturbed sediment core (Golcuk18-P01) was recovered in September 2018 at a water depth of 22 m in the N-NE part of Lake Gölcük using a piston sediment corer. The core was split lengthways into halves. One half was used for sample selection and preparation for lithological description (at mm scale), stable isotope analyses ($\delta^{18}O$ and $\delta^{13}C$), and ^{14}C dating, whereas the other half was used for scanning for magnetic susceptibility and µXRF elemental analysis.

Elemental analysis was carried out at the Istanbul Technical University (ITU) East Mediterranean Centre for Oceanography and Limnology (EMCOL) using molybdenum tube embedded in Itrax core scanner. The scanner can measure elements ranging from Al to U, as well as radiography of cores (Croudace et al., 2006, 2019). The core Golcuk18-P01 was scanned at 1-mm intervals using a scan time of 30 seconds with current of 10 kV and 0.3 mA. Although the analysis was carried out at 1-mm intervals, the results were averaged to 5-mm intervals for noise reduction and better visual correlations. The radiography also was measured using the same equipment.

The elemental results of Fe, Ti, Ca, Mn, Sr, and K obtained from µXRF analysis were subjected to factor analysis. However, since µXRF counts conform to compositional statistics (Weltje and Tjallingii, 2008), data transformation and outlier removal were conducted prior to the factor analysis. The *outCoDa* function, a robust outlier detection approach (Filzmoser and Hron, 2008), was employed for this purpose. This function is part of the *robcompositions* package (Filzmoser et al., 2018; Reimann et al., 2008) in R (R Core Team, 2021). The factor analysis algorithm described by Fizmoser et al. (2009), which utilizes the principal factor analysis of centered log-ratio transformed data, was applied using the *pfa* function in the *robcompositions* package in R.

Magnetic susceptibility (MS) analysis was carried out using Bartington point sensor embedded in a Geotek Multi Sensor Core Logger (MSCL) (Weber et al., 1996), which is also located
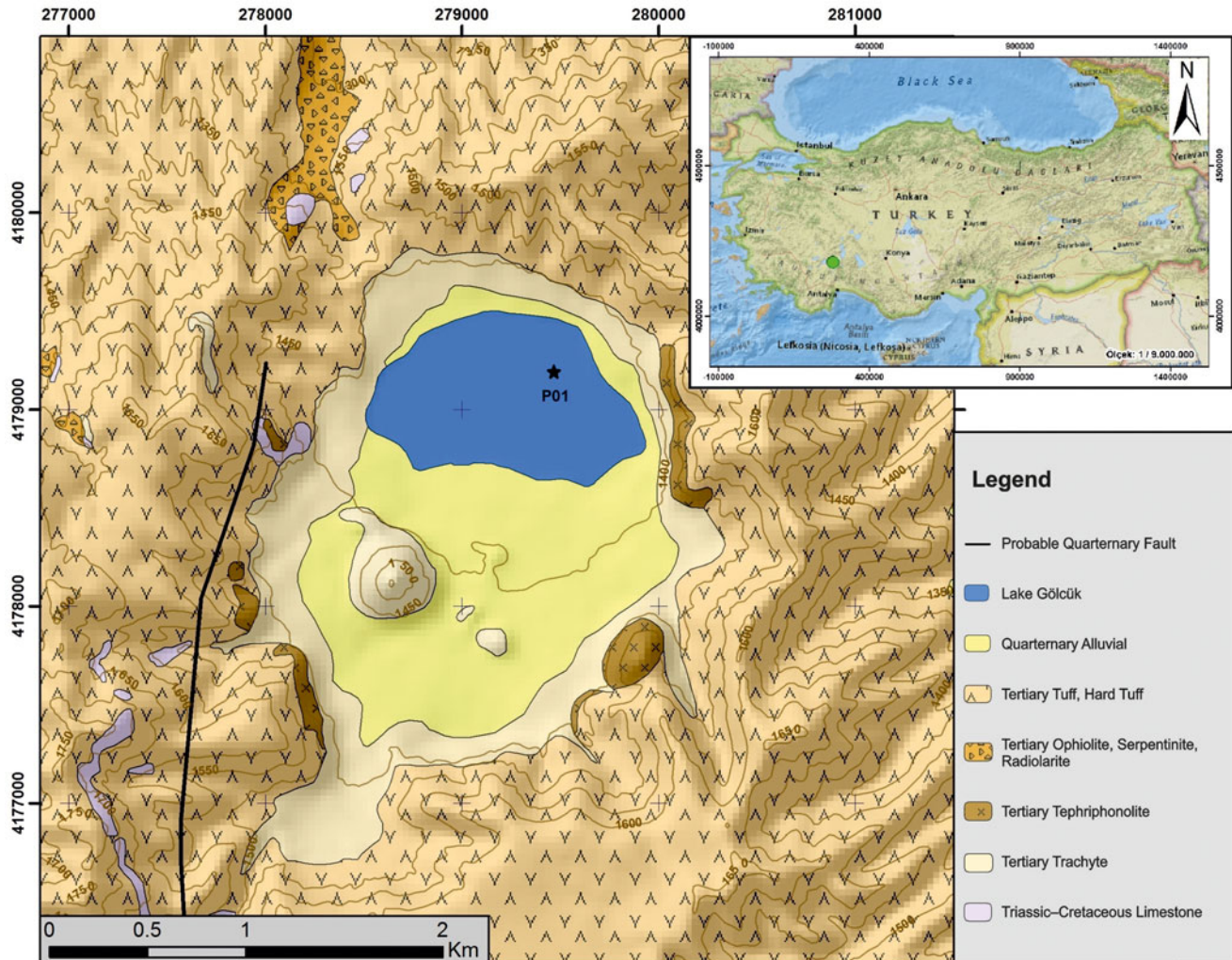
Figure 1. Location map of Lake Gölcük (green dot) together with the regional geology. The location of the drilled core is indicated with a black star.

at the ITU-EMCOL laboratory. The analysis was carried out at 5-mm intervals.

Fifty samples were selected at ~2.5-cm intervals for $\delta^{18}O$ and $\delta^{13}C$ analyses. The samples were cleaned of impurities by washing with water and 63-μm sieving. Light microscope was then used for selecting the shells of *Candona neglecta*, which is the most abundant and available ostracod species throughout the core. The samples were then analyzed using the normal procedure for $\delta^{18}O$ and $\delta^{13}C$ at the Environmental Isotope Laboratory, University of Arizona Tucson (Bar-Matthews et al., 1998; Roberts et al., 2008).

Sediment samples measuring 4 cm³ were collected at ~2.5-cm intervals from the P01 sediment core. In total, 50 sediment samples were collected for pollen analysis. Using the standard pollen preparation procedure of Faegri and Iversen (1989), the samples were analyzed through the chemical and sieving procedure. As a marker for absolute pollen and non-pollen palynomorph concentrations, a lycopodium tablet was added (Stockmarr, 1971). The pollen diagrams and stratigraphic cluster analysis were evaluated using Tilia software (Grimm, 1987).

AMS ^{14}C analyses of seven samples, which included both ostracod shells and organic carbon, were carried out in different laboratories (see Table 1 for details). The laboratory in which the analyses were carried out and number of samples dated (in

parentheses) are as follows; Beta Analytic (1), ETH Zurich (5), and Poznan (1). The AMS ^{14}C dating at the Poznań Radiocarbon Laboratory in Poland was carried out on the organic remains in the sediments. On the other hand, the analyses at Beta Analytic USA and ETH Zurich Switzerland were made on ostracod shells using standard AMS ^{14}C and Mini Carbon Dating

Table 1. ^{14}C laboratory (uncalibrated) results of core Golcuk18-P01 showing Lab ID, age (BP), depth (cm), and dated materials.

Lab ID	Age (BP)	Depth (cm)	Materials
ETH.96336.1.1	589 ± 131	32.5	Ostracod shells
Poz-112573	555 ± 30	55.5	Organic materials (Bulk)
ETH.96337.1.1	885 ± 64	75.5	Ostracod shells
ETH.96338.2.1	1209 ± 64	92.5	Ostracod shells
ETH.96340.1.1	1264 ± 50	143	Ostracod shells
ETH.96340.2.1	1289 ± 64	143	Ostracod shells
Beta.509396	1440 ± 30	196	Ostracod shells

System (MICADAS) methods, respectively. The rationale for using the MICADAS method (ETH Zurich) is because the amount of ostracod in the 5 samples was lower (<5 mg) compared to the amount of ostracod sample (≥10 mg) required for dating at Beta Analytic USA.

RESULTS

Chronology

The age-depth model was reconstructed using a Bayesian procedure implemented in the *rbacon* package in R (Blauw and Christen, 2011). Calibration of each radiocarbon date was conducted using the IntCal13 curve (Reimer et al., 2013) within the same package to take advantage of the full form of the curve as a prior distribution in the stochastic process of the *rbacon* package. Since the approach is Bayesian, it requires incorporation of prior assumptions expressed as probability distributions in the model. The model assumes a gamma distribution to describe the core's accumulation rate and a beta distribution for the memory of the accumulation. The parameters selected for the gamma and beta distributions were $(\alpha,\beta) = (1.5,10)$ and $(\alpha,\beta) = (4,0.7)$, respectively. According to our age-depth model, Golcuk18-P01 covers approximately the last 1550 cal years BP (see Fig. 2).

The mean uncalibrated ages of samples taken from depths of 32.5 cm and 55.5 cm in the core are almost identical, with the latter date being slightly younger (Table 1). It should be noted that the laboratories and dated materials used for each depth were different: ostracod shells were analyzed at 32.5 cm and bulk material at 55.5 cm. The apparent inconsistency may be due to variations in analytical procedures, specifically the use of different laboratories or materials during the analyses. However, the calibrated age ranges show that the 2σ uncertainty intervals are consistent with the depths of the dates. The vertical blue bulbs in Figure 2 represent the probability distributions of calibrated ages at each depth, where the distribution at 32.5 cm elongates down to the distribution at 55.5 cm.

Factor Analysis

Factor analysis revealed three groups of elements that correspond to an elemental variance of 74% (Table 2). The first group was represented by K and Ti; the second group was represented by Mn and Fe; and the third group was represented by Ca and Sr (Fig. 3).

Abiotic Proxies

The lithology of core Golcuk18-P01 between AD 450–730 is characterized by homogeneous mud lithology (Fig. 4). Between AD 730–810, sandy lithology is noted, followed by mud lithology from AD 810–880. Below AD 880 re-emergence of sandy lithology dominated until AD 1400. Finally, the lithology shows a prevalence of silty mud until AD 2018.

The radiography results on the other hand suggest a generally light radiography between AD 450–750 (Fig. 4). From AD 750–1000, dark radiography is observed, which is followed by a light radiography until AD 1150. Between AD 1150–1600, a generally dark radiography prevailed, followed by a light radiography until AD 2018.

The MS documented relatively low values from AD 450–730, followed by high values between AD 730–810 (Fig. 4). Conversely, relatively high MS values persisted between AD 730–810. Reaching AD 880, relatively low values were observed. The MS values between AD 880–1400 were relatively high, with exception of the values from AD 1000–1150. From AD 1400–2018, the MS documents relatively low values.

Isotopes of $\delta^{13}C$ and $\delta^{18}O$ between AD 450–730 show relatively elevated values, which are followed by relatively depleted values between AD 730–810 (Fig. 4). From AD 810–880, the $\delta^{13}C$ and $\delta^{18}O$ revealed relatively high values, followed by relatively low values between AD 880–1400. However, interruption from relatively low values were documented from AD 1000–1150. Between AD 1400–2018, the $\delta^{13}C$ and $\delta^{18}O$ data indicate generally relatively low values, except for AD 1450–1550, AD 1645–1715, and AD 1790–1820 periods.

Low values of log(Ca/K) were recorded in the period AD 450–730, followed by relatively high values between AD 730–810
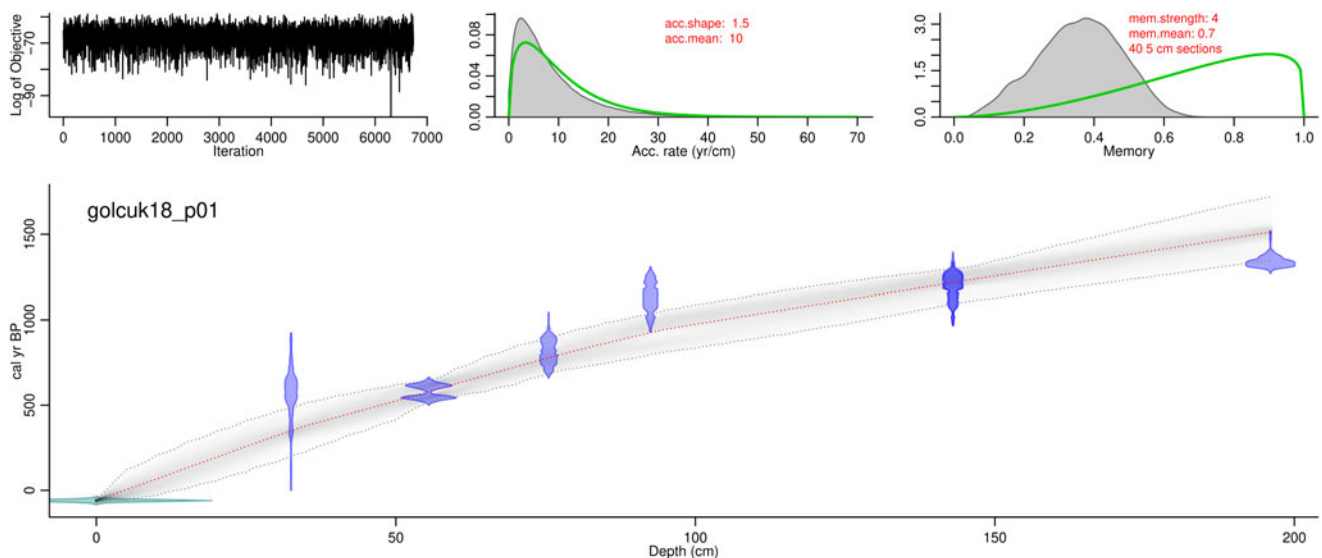

Figure 2. The age-depth model of the Golcuk18-P01 core reconstructed from seven ^{14}C dates. Top panel, from left to right: trace plot of Markov chain Monte Carlo (MCMC) runs of the log-posterior distribution (left), prior (green), and posterior (shaded) distributions for accumulation rate and the memory models. Below, the age depth model is given and the 95% confidence intervals for all depths are shown as gray shade. The blue shapes represent the vertically mirrored probability distribution of each calibrated date.

Table 2. The results of the factor analysis showing three factors (groups of elements). Lower panel shows the proportional variance explained by each factor and cumulative variance i.e. summation of proportional variances that show the percentage of the total variance explained by the extracted factors.

	Factor 1	Factor 2	Factor 3
K	**0.845**	−0.025	0.064
Ti	**0.734**	0.239	0.221
Mn	−0.059	**0.875**	0.017
Fe	0.449	**0.758**	−0.015
Ca	0.421	0.065	**0.712**
Sr	−0.017	−0.013	**0.893**
Proportional variance	0.273	0.236	0.231
Cumulative variance	0.273	0.509	0.740

(Fig. 4). In the period AD 810–880, relatively low log(Ca/K) values were documented. On the other hand, the period AD 880–1400 generally documents relatively high values, except for AD 1000–1150. From AD 1400–2018, the log(Ca/K) data have relatively low values.

Biotic proxies

High percentages of herbaceous (*Artemisia* and *Poaceae*) taxa between AD 450–750 (196–130 cm), followed by relatively higher trees and shrubs from AD 750–950 (130–105 cm) were documented. The tree taxa are mainly represented by *Pinus* and to a lesser extent *Juniperus* type, *Quercus* (deciduous), and *Quercus* (evergreen). Based on Lake Gölcük's pollen record, *Artemisia* was the most abundant taxon followed by *Poaceae* in the steppe vegetation (Fig. 5). The percentage of Cerealia is low. with an average of 2.3%. The pollen concentration in this zone is high.
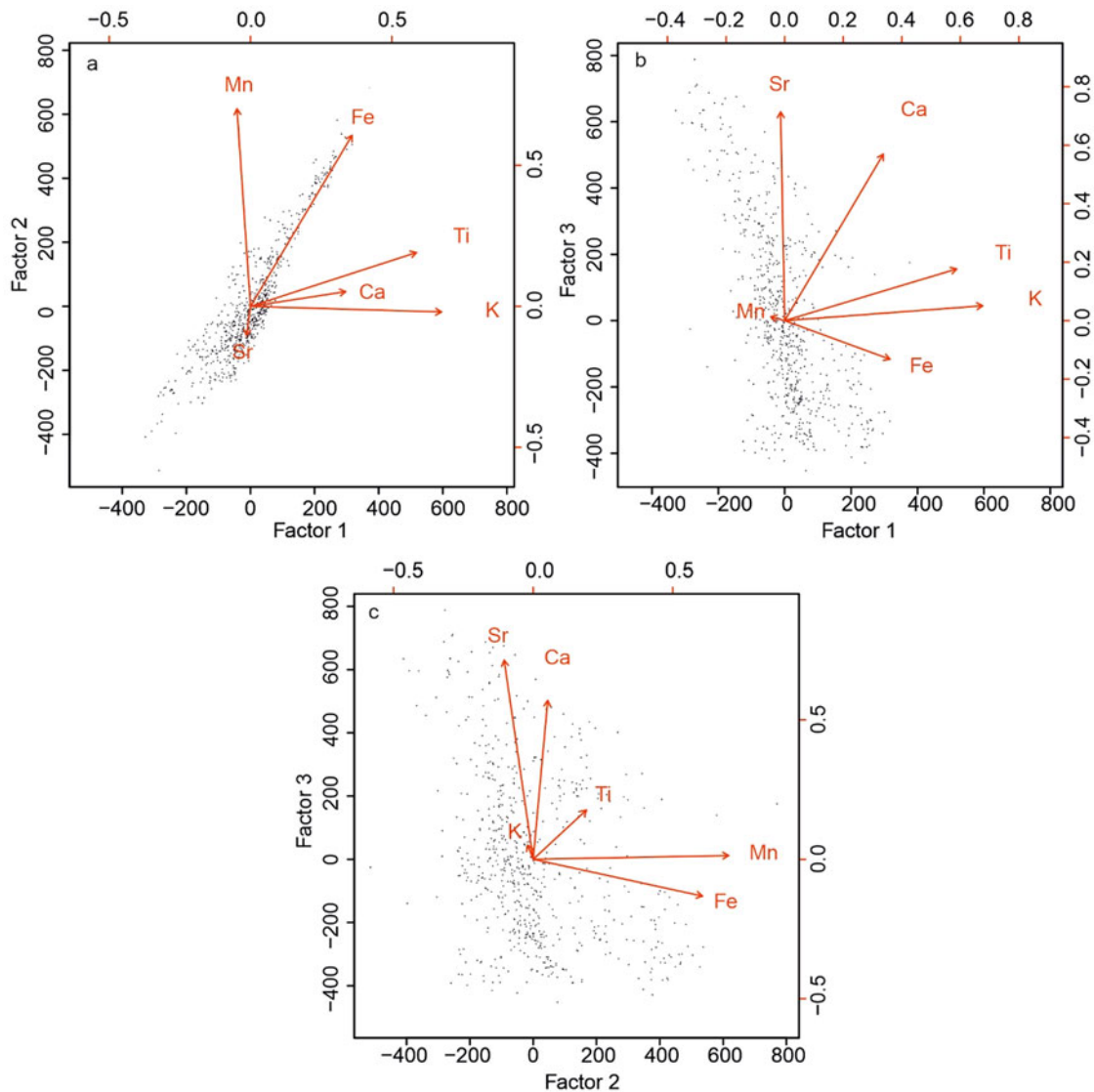

Figure 3. Biplots depicting the three factors resulting from robust factor analysis for centered log-ratio transformed X-ray fluorescence (µXRF) counts of Mn, Fe, K, Ca, Ti, and Sr. The plots illustrate the relationships among the variables and factors, with each arrow representing a variable and the angle between pairs of arrows indicating the strength and direction of the relationship. The factors are labeled according to the main variables that contribute to them, and can provide insights into the underlying patterns and sources of variation in the µXRF data.
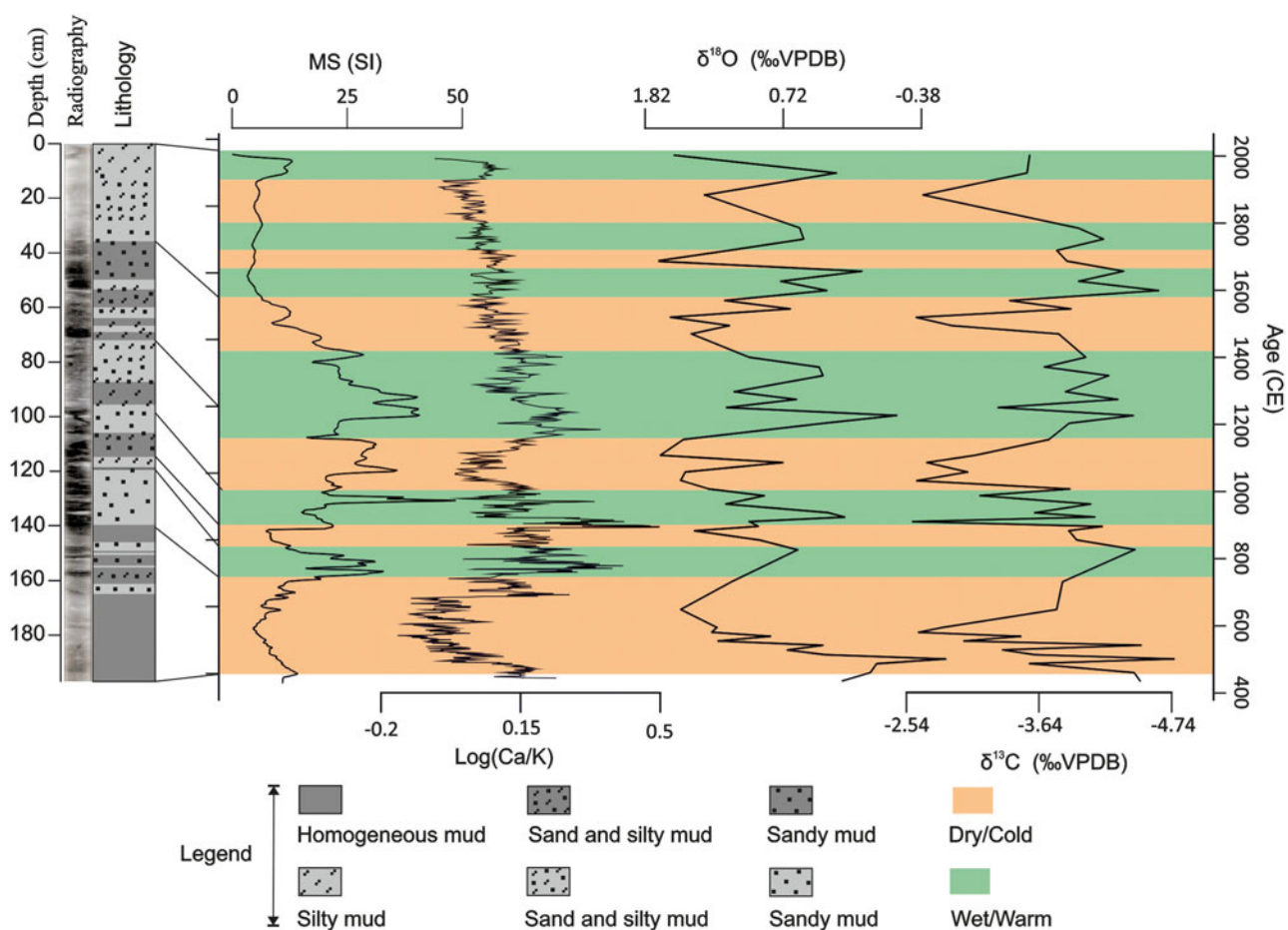
Figure 4. Plot of the multiproxy results of the Lake Gölcük P01 record. From left to right; radiography measurement of the core from micro XRF, lithological description, magnetic susceptibility measurement (MS), log ratio of Ca to K, ∂^{18}O, and ∂^{13}C. VPDB = Vienna Pee Dee Belemnite.

From AD 750–950 (130–105 cm), the percentage of the herbaceous (*Artemisia* followed by *Poaceae*) taxa declined, whereas the trees slightly increased. Conifers (*Pinus*, *Juniperus*), *Quercus* (deciduous), and *Quercus* (evergreen) all increased. In this period, a relatively high pollen concentration in the pollen assemblage zone was observed.

From AD 950–1220 (105–60 cm), *Artemisia* followed by *Poaceae* dominated the steppe elements. The trees in the pollen assemblage (*Pinus*, *Juniperus*, *Quercus* [deciduous], and *Quercus* [evergreen]) were reduced. *Plantago* and Cerealia increase slightly.

From AD 1410–2018 (50–0 cm), herbaceous taxa (mainly *Artemisia* and *Poaceae*) increased, whereas the tree pollen (*Pinus*, *Juniperus*, *Quercus* [deciduous], and *Quercus* [evergreen]) declined.

DISCUSSION

Mn, Fe, Ti, and K are siliciclastic components of lakes, which are commonly derived from the lake surroundings (Cohen, 2003; Croudace et al., 2019). However, Ca and Sr may not only be derived from the lake surrounding but also form within the lake system and are widely regarded as endogenic components (e.g., Davies et al., 2015). In Lake Gölcük, the siliciclastic components are derived from volcanics, which are rich in Mn, Fe, Ti, and K. But the factor analysis results suggest loading of Mn and Fe in group one, whereas Ti and K loaded in group two. This can

be seen as a contradiction to our interpretation. However, given the redox behavior of both Mn and Fe, one can suspect the redox behavior of Fe and Mn in lake systems to be the reason (Cohen, 2003; Żarczyński et al., 2019). Nevertheless, the correlation between the two groups is positive (Fig. 3), meaning both group 1 and 2 are from siliciclastic components. For Sr and Ca, the factor analysis suggests loading in group three, which is interpreted as endogenic components because they are neither positively correlated with group 1 nor with group 2. It is acknowledged that stating the exact source of Ca and Sr based on the current proxy can be problematic, as a result, it is assumed to be precipitated and/or biotic in origin.

The lithological changes in the Lake Gölcük P01 core indicate varying sediments deposited due to three agents: mass wasting (seismic activities), varying climate, and/or changes within the lake system. Mass wasting can be easily identified by observing sediment sorting in core sediments, which was not observed in the P01 record. Although evidence based on a single proxy can be misleading, no reversal in the radiocarbon dates that would indicate sediment mixing due to mass wasting was encountered. Based on these lines of evidence, mass wasting is ruled out and energetic (non-energetic) environments is proposed, possibly during wet (dry) periods, as the reason for varying lithology in the lake. The interpretation of energetic (non-energetic) environments is supported by dark (light) radiography image. Dark radiographic images in core sediments usually represent
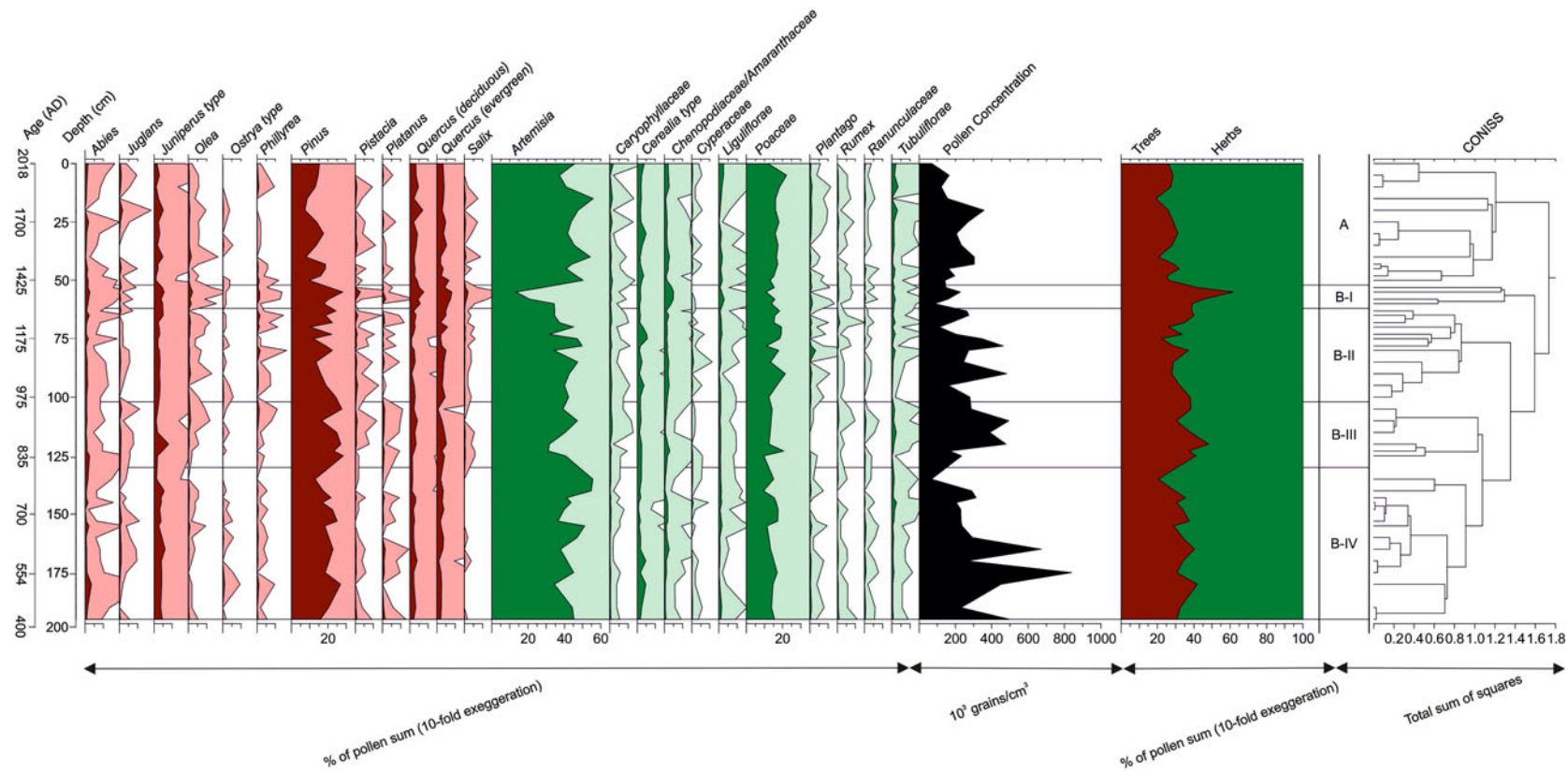
Figure 5. Pollen diagram of Lake Gölcük core P01 plotted against depth with most abundant taxa, pollen concentrations, percentage of trees, shrubs, and herbs, LPAZ (local pollen assemblage zones), and cluster analysis.

accumulated coarser-grained sediments in lake systems due to precipitation (Danladi and Akçer-Ön, 2018). On the other hand, light radiography reflects more fine-grained sediments that accumulated in a more stable, or dry climate period.

The log(Ca/K) reflects calcite versus siliciclastic inputs and can be interpreted as precipitated calcite in the lake system. The justification is that warm summer temperatures lead to increase in precipitated calcium in water column. In fact, Danladi et al. (2021) found the log(Ca/K) in Lake Gölcük to be a direct proxy for summer temperature. MS is a proxy for siliciclastic materials entering lacustrine environments and its high (low) values usually suggest high (low) input of siliciclastic materials in a lake (Thompson et al., 1976). The siliciclastic materials migrate into the lake due to precipitation, mass wasting, or reduced lake water level in a lacustrine environment. Since there is no evidence of mass wasting in the Lake Gölcük core, the MS record is interpreted as a proxy for wet/dry periods. $\delta^{13}C$ and $\delta^{18}O$ isotopes in closed basins are interpreted as proxies for precipitation/evaporation. The justification is fractionation processes of $\delta^{13}C$ and $\delta^{18}O$, which are controlled by the precipitation/evaporation ratio (Li and Ku, 1997; Roberts et al., 2008).

Increase in tree pollen is often associated with increased moisture, whereas the prevalence of steppe vegetation is linked to decrease in moisture or increase in human activities (England et al., 2008; Bakker et al., 2012; Şenkul et al., 2018). Such human activities could be related to land clearance for agricultural and/or settlement purposes. Evidence of land clearance is often associated with decrease in woodlands. In Lake Gölcük the increase/decrease in tree pollen can be ascribed to increase/decrease in moisture because of several reasons: (1) tree pollen increase is often associated with increase in conifers followed by *Juniperus* type and *Quercus* (evergreen and deciduous); (2) the overall high concentration of pollen indicates the prevalence of well-vegetated land cover; and (3) the low amount of anthropogenic indicators such as *Cerealia*, and in some cases herbs such as *Chenopodiaceae/Amaranthaceae*, also increase with climate improvement.

LAKE GÖLCÜK CLIMATE CHANGE THROUGH TIME

Dark Ages Cold Period (DACP: AD 450–750)

The homogeneous mud lithology in the Lake Gölcük P01 core between AD 450–750 indicates a dry climate contributing to the accumulation of mud materials. Similarly, the light radiography image suggests low siliciclastic input. This agrees with low value of MS reflectance, which suggests less magnetic siliciclastic materials entering the lake (Thompson et al., 1976). The relatively high $\delta^{13}C$ and $\delta^{18}O$ values between AD 450–730 imply dry climate conditions (Li and Ku, 1997; Roberts et al., 2008). The low log(Ca/K) values during this period indicate cold climate conditions (Danladi et al., 2021). Also supporting the multiproxy interpretation during this period, the dominance of *Artemisia* and *Poaceae* and low tree pollen (*Pinus*, *Juniperus* type, *Quercus* [deciduous and evergreen]) suggest the prevalence of steppe vegetation under dry climate conditions. The low amount of *Cerealia*-type vegetation (average 2.3%) during this period suggests that the taxa probably are not cultivated, but growing on their own (Zeist et al., 1975).

Comparison of the multiproxy record with local climate data reveals a general climate pattern (Fig. 6). At Lake Beyşehir, a period of reduced conifers and increased herbaceous pollen (mainly *Artemisia* and *Chenopodiaceae*) was recorded between AD 400–750 (Zeist et al., 1975). $\delta^{18}O$ of Kocain Cave data suggest dry climate conditions between ca. AD 460–830 (Jacobson et al., 2021). A similar dry period is recorded from AD 600–770 in Ca/Fe data from SW Anatolian Lake Salda (Danladi and Akçer-Ön, 2018). Similarly, dry climate conditions are evidenced by a shift from crop cultivation to pastoralism in Gravgaz Marsh of SW Turkey from AD 650–940 (Bakker et al., 2012). However, Lake Burdur, also in SW Anatolia, records wet climate conditions during this period (Tudryn et al., 2013). The deviation of results between Lake Burdur and SW Anatolian lakes Beyşehir, Salda, and Gölcük may be associated with age-related issues because the former is better age constrained than the latter.

In Central Anatolia, the pollen records of Lake Nar suggest a period of elevated grass pollen from AD 450–670 (England et al., 2008), whereas the $\delta^{18}O$ of this lake suggests wet climate conditions (Jones et al., 2006). As a result, England et al., 2008, suggested that climate change may not be a direct vegetation driver in the Lake Nar vicinity. In the eastern Anatolian Lake Van, dry and cold climate conditions were documented from AD 650–950 (Barlas Şimşek and Çağatay, 2018). Increased *Pinus* and *Ranunculaceae* pollen in Central Anatolian Lake Tuzla suggest a wet climate at Lake Tuzla between AD 40–835 (Şenkul et al., 2018). In NW Anatolia, the $\delta^{18}O$ record of Lake Çubuk and $\delta^{13}C$ of Sofular Cave suggest wet climate conditions between ca. AD 500–730 (Göktürk et al., 2011; Ocakoğlu et al., 2016). Therefore, it broadly appears that cold and dry conditions prevailed during the DACP in SW Anatolia, whereas wet conditions occurred in central and northern Anatolia.

In EM, multiproxy analyses of a sediment core suggest dry climate conditions from AD 350–650 in the Gulf of Saros (NE Aegean Sea) (Bozyiğit et al., 2022). In contrast, paleoclimate records from Lake Stymphalia in Greece suggest cooler temperature from AD 400–500 (Seguin et al., 2019). In the central Mediterranean, $\delta^{18}O$ and $\delta^{13}C$ planktonic foraminifer studies in the Gulf of Toronto suggest wet climate conditions from AD 500–750 (Grauel et al., 2013). During a similar period, cold climate conditions were documented by stalagmite records in the central Mediterranean (Frisia et al., 2005). In their synthesis of contemporary Mediterranean and European regional studies, Helama et al. (2017) suggested widespread prevalence of dry climate conditions during the DACP. Within the DACP timeframe, a period of cold climate from AD 536–660 has been referred to as the Late Antique Little Ice Age (LALIA; Büntgen et al., 2016). The LALIA is of particular interest to climate scientists and historians interested in testing and building hypotheses about climatic-societal links (Haldon, 2016).

Medieval Climate Anomaly (MCA: AD 950–1250)

From AD 950–1220, the sandy lithology implies wet climate during this period. This is also evidenced in the dark radiography image indicating wet climate condition.

The mostly sandy lithology during this period implies an energetic environment (precipitation) leading to the deposition of coarse-grained sediments. Accordingly, the MS, $\delta^{13}C$, and $\delta^{18}O$ suggest an increase in precipitation, albeit with interruption of a dry period between AD 1000–1150. MS data also increase between AD 1000–1150 suggesting a probable wet period and thus, a contradiction. The contradiction can be explained by the increase in erosion of terrestrial materials possibly due to a dry period that resulted in low water level. On the other hand, the generally relatively high Ca/K suggests an increase in carbonate
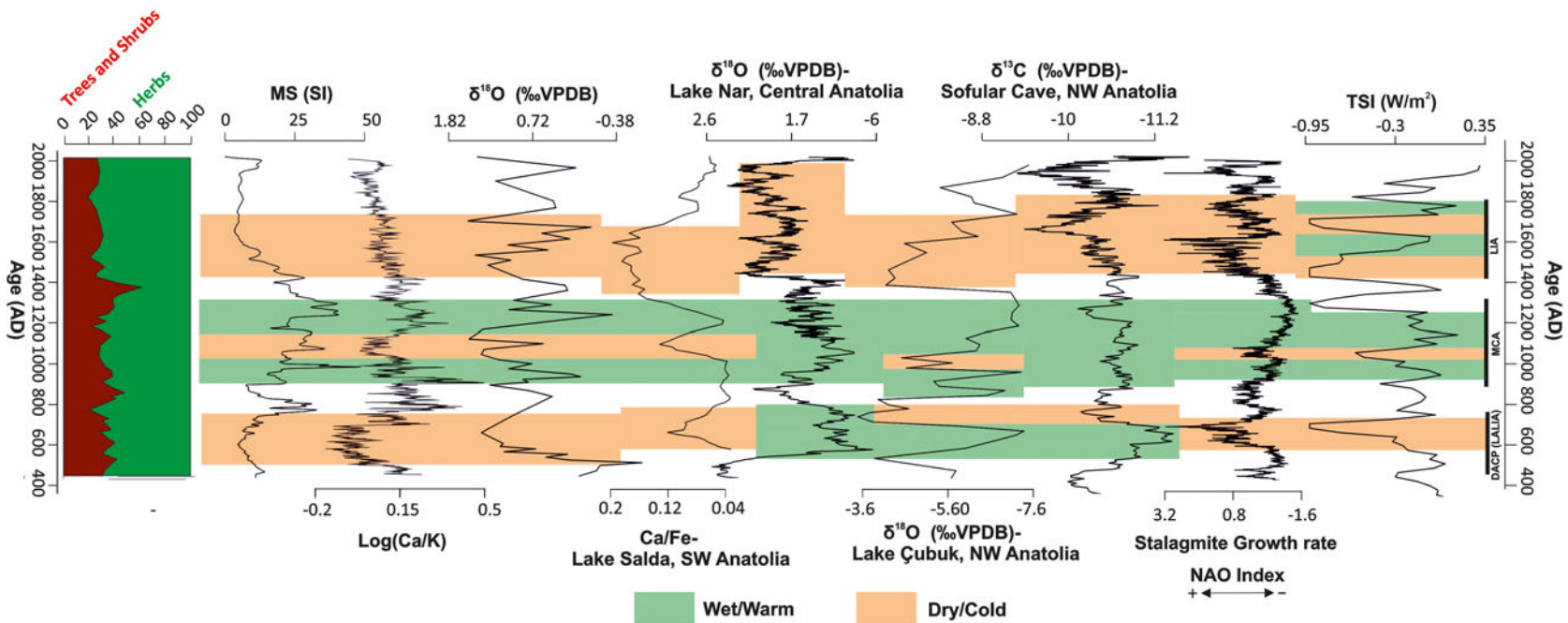
Figure 6. Side-by-side comparison of the Lake Gölcük proxies to contemporary Anatolian records from Lake Salda (Danladi and Akçer-Ön, 2018), Lake Nar (Jones et al., 2006), Lake Çubuk (Ocakoğlu et al., 2016), and Sofular Cave (Göktürk et al., 2011), stalagmite growth rate (NAO) (Baker et al., 2015), and TSI (Delaygue and Bard, 2011). DACP = Dark Ages Cold Period; LALIA = Late Antique Little Ice Age; LIA = Little Ice Age; MCA = Medieval Climate Anomaly; VPDB = Vienna Pee Dee Belemnite.

precipitation due to an increase in summer temperature. Conversely, relatively low Ca/K between AD 1000–1150 suggests a decrease in carbonate precipitation due to a decrease in summer temperature. During period between AD 950–1250, steppe vegetation dominated, albeit with continuous interruption by tree pollen. However, we cannot clearly see the dry period between AD 950–1250, possibly because of proxy sensitivity. In the herbaceous pollen, *Artemisia* followed by *Poaceae* dominated the steppe elements. For the tree pollen, the main fluctuations involved conifers (mainly *Pinus*), followed by *Quercus* (deciduous) and *Quercus* (evergreen). The secondary anthropogenic indicator, *Plantago*, followed by the primary anthropogenic indicator, *Cerealia*, both show slight increases, suggesting either cultivation or taxa response to climate amelioration.

The proposed climate reconstruction in this study is similar to the wet climate condition (AD 900–1000) followed by dry climate (AD 1000–1150) and wet climate (AD 1150–1250) in Lake Salda (Danladi and Akçer-Ön, 2018) (Fig. 6). In Gravgaz Marsh, wet climate conditions and the re-emergence of human activity were recorded from AD 940–1280 (Bakker et al., 2012). Contrary to the SW Anatolian records, the δ¹⁸O of Kocain Cave suggested a rather dry climate from AD 850–1300 (Jacobson et al., 2021). In Central Anatolia, reduced arboreal pollen in Lake Tuzla suggests dry climate conditions between AD 830–1100 (Şenkul et al., 2018). Cereal farming, pastoralism, and steppe elements were recorded between AD 950–1090 in Cappadocia (England et al., 2008). However, the δ¹⁸O data from Lake Nar suggest wet climate conditions from AD 1000–1400 (Jones et al., 2006). In the eastern Anatolian Lake Van, wet and warm climate conditions were documented from AD 950–1250 (Wick et al., 2003; Barlas Şimşek and Çağatay, 2018). In NW Anatolia, during the period between AD 900–1250, the δ¹⁸O record of Lake Çubuk suggests a generally wet climate, which is interrupted by a dry climate ca. AD 1000 (Ocakoğlu et al., 2016). Similarly, the Sofular Cave record of δ¹³C suggests wet climate conditions between AD 900–1200 (Göktürk et al., 2011).

In the Mediterranean region, paleoclimate records suggest a generally opposite climate between the EM and the western Mediterranean (WM). In the EM region, a paleoclimate record in the NE Aegean suggests wet climate conditions (Bozyiğit et al., 2022). Similarly, a record from Lake Stymphalia in neighboring Greece showed increase in terrigenous elements from AD 1000–1400, suggesting wet climate conditions (Seguin et al., 2019). In Israel, high water levels were reported from AD 1100 to ca. AD 1300 (Bookman et al., 2004). In the WM, several studies from the Iberian Peninsula and Morocco reported a rather cold and dry climate period, which is opposite of the EM climate (Roberts et al., 2012; Ait Brahim et al., 2017; Lüning et al., 2019). This East-West climate dipole has been previously ascribed to the NAO and its influences through the westerlies (Lüning et al., 2018; Roberts et al., 2012). In the Levant, cyclogenesis together with topographical differences were attributed to precipitation changes (Kushnir and Stein, 2010). In Europe, warmer and wetter climate conditions attributed to the NAO were documented by paleoclimate records from AD 950–1250 (Andres and Peltier, 2016; Mann et al., 2009). In fact, the MCA is thought to be comparatively warmer and wetter than the current warm period (Mann, 2002; Musk, 1980).

Little Ice Age (LIA: AD 1250–1850)

Between AD 1400–1850, the lithology shifted from sandy to mostly silty and muddy, suggesting a shift towards drier climate

conditions. Similarly, the light radiography image suggests low terrestrial input, which resulted from drier climate conditions. Accordingly, relatively low MS suggests a reduction in terrigenous supply owing to reduced precipitation. During the same period, the δ¹³C and δ¹⁸O data have relatively low values, except for AD 1450–1550, AD 1645–1715, and AD 1790–1820, implying increased P/E ratio because of high evaporation. These exceptional periods, AD 1450–1550, AD 1645–1715, and AD 1790–1820, with relatively high values suggest a reduction in the P/E ratio owing to increase in precipitation. However, MS and log (Ca/K) did not capture these changes, implying possible differences in proxy sensitivity or that a possible change in lake chemistry occurred. These dry periods may be related to periods of reduced solar activity (Spörer Minimum: Jiang and Xu, 1986; Maunder Minimum: Eddy, 1976; Dalton Minimum: Wagner and Zorita, 2005). From AD 1250–1850, a shift from high tree pollen to high herbaceous pollen is recorded, which suggests a climate shift from wetter to drier conditions. Most of the changes were captured by the conifers (mainly *Pinus* followed by *Juniperus* type) and oak trees (*Quercus* [deciduous] and *Quercus* [evergreen]). Conversely, steppe elements are evident in the herbaceous taxa (mainly *Artemisia* and *Poaceae*).

In Lake Salda, generally dry climatic conditions were recorded from AD 1400–1850 (Fig. 6). Similarly, dry climate conditions, evinced by low lake water level, were reported in Lake Burdur (Tudryn et al., 2013). In Gravgaz Marsh, dry climate conditions and reduced cereal cultivation were evident from AD 1280 (Bakker et al., 2012). Contrary to our record and the other records in SW Anatolia, the record of Kocain Cave suggests wet climate conditions during the period AD 1400–1700 (Jacobson et al., 2021). In Central Anatolia, the Lake Nar δ¹⁸O data suggest a shift towards dry climate from AD 1400–1850 (Jones et al., 2006). Similarly, the δ¹⁸O data in Lake Tecer (Central Anatolia) record dry climate conditions between AD 1400–1800. The δ¹³C data of Sofular Cave only record a dry climate from AD 1600–1700.

In the EM, the paleoclimate record in the NE Aegean suggests dry climate conditions from AD 1220–1840 (Bozyiğit et al., 2022). On the coast of Syria, dry and cold climate conditions have been documented from AD 1520–1870 (Kaniewski et al., 2011). Similarly, data from Lake Stymphalia in Greece suggest an unstable climate condition that might have resulted in drying of the lake (Seguin et al., 2019). However, the record from Etiliko Lagoon suggests climate amelioration, possibly because the latter was in a coastal region or because of proxy responses (Koutsodendris et al., 2017). In Israel, dry climate conditions are suggested by δ¹⁸O data from the Ashdod Coast (Schilman et al., 2002). In the WM region, wetter and warmer climate conditions have been documented in Iberian Peninsula and Morocco (Abrantes et al., 2017; Ait Brahim et al., 2017).

CLIMATE MECHANISMS

To understand the climate drivers and mechanisms, the record in this study was compared to the NAO index (Baker et al., 2015) and Total Solar Irradiance (TSI) data (Delaygue and Bard, 2011) (Fig. 6). The comparison shows that all the dry (wet) periods in the Lake Gölcük record are correlated with NAO+ (NAO−), suggesting that precipitation in the region was controlled by NAO. With a pressure difference between the Icelandic high and sub-polar low, the NAO is reported to be the largest atmospheric circulation in the North Atlantic (Cullen and

deMenocal, 2000). NAO influence is exerted through the jet stream and storm tracks, which transport the energy for major changes in precipitation and temperature. Depending on the pressure differences, NAO−/NAO+ southward/northward displacement of the storm tracks occur. During the NAO−, increases in storms and low-pressure systems lead to higher precipitation in Anatolia, resulting in above-average rainfall (Kahya, 2011). Whereas the NAO+ results in weak trade winds and consequently fewer storms, which result in lower-than-normal precipitation. A number of EM studies had reported the NAO as an important contributor of winter moisture (Cullen and deMenocal, 2000; Jones et al., 2006; Luterbacher et al., 2012; Danladi and Akçer-Ön, 2018). In fact, the NAO is not only important for the formation of winter climate of the EM, but also for the whole Mediterranean region. Furthermore, a dipole pattern of the NAO has been observed between the EM and the WM (Roberts et al., 2012; Lüning et al., 2019). For instance, Roberts et al. (2012) observed that NAO− (NAO+) was associated with wet (dry) periods in the EM and the opposite for the WM. This is also confirmed by a recent literature compilation (Lüning et al., 2019) stating that the situation exists even for paleotemperature variations. However, reduced correlation between precipitation and NAO towards the Levant has been suggested (Cullen and deMenocal, 2000; Enzel et al., 2003). Following this assertion, Kushnir and Stein (2010) explained that precipitation changes in the Levant are related to cyclogenesis (Cyprus Lows), which formed due to the encounter of cold pressure systems from Europe with warm sea surface of the EM.

It is also important to note that other atmospheric circulation patterns, such as the East Atlantic or the North Sea–Caspian pattern, have been suggested previously in contemporary Anatolian and EM studies (Kutiel et al., 2002; Touchan et al., 2005; Jones et al., 2006). For example, at Lake Nar (Central Anatolia) and Lake Salda (SW Anatolia), possible influence of the NCP was suggested for Late Holocene paleoclimate reconstructions (Jones et al., 2006; Danladi and Akçer-Ön, 2018). However, the East Atlantic/Western Russia pattern was suggested for Lake Tecer (Central Anatolia) during the Middle–Late Holocene (Kuzucuoğlu et al., 2011).

Comparison of the Lake Gölcük record to TSI (solar activity proxy) revealed that all the dry (wet) periods are correlated with low (high) TSI data. Several studies previously had recorded a close link between NAO phases and solar activity (Thiéblemont et al., 2015; Yukimoto et al., 2017). These studies suggested a possible medium in the stratosphere through which the phases of NAO were categorically modulated by solar activity. Because high (low) TSI in the Lake Gölcük record corresponds to wet (dry) periods, these climate changes may have been caused by solar activity, possibly through solar influence on mid-latitude westerlies. Danladi et al. (2021) previously had demonstrated, through instrumental data and a 300-year paleoclimate reconstruction, that the Lake Gölcük climate changes are directly influenced by the TSI. Accordingly, the influence of solar activity on paleoclimate records has been observed in SW Anatolian Lake Salda (Akçer Ön, 2017; Danladi and Akçer-Ön, 2018), Lake Köyceğiz (Akçer Ön, 2017), and a tree-ring reconstruction in Antalya (Heinrich et al., 2013). In the EM, similar solar influence also has been recorded in paleoclimate records of neighboring Greece (Koutsodendris et al., 2017). Similarly, a review article of the EM and Mesopotamia by Kushnir and Stein (2019) suggested an antithetical relationship between paleoclimate records and solar activity. In the WM, the influence of solar activity also has

been documented (Koutsodendris et al., 2017; Brahim et al., 2018). In addition, an increasing number of climate models provide some evidence through which solar activity affects climate (Swingedouw et al., 2011; Yukimoto et al., 2017; Hernández et al., 2020). Through a medium in the troposphere, these studies suggest that solar activity results in a shift in the state of the North Atlantic Oscillation (NAO), thereby resulting in NAO+(NAO−) conditions, which is later translated into precipitation/temperature changes in climate in the North Atlantic, Eurasia, and the Mediterranean regions (Kahya, 2011; Thiéblemont et al., 2015).

CONCLUSIONS

The results of this study show the relationship of climate variability and the imprint of regional climate change at Lake Gölcük (SW Anatolia) through several climate periods since ca. AD 400 (1550 cal years BP). The lithology, radiography, MS (SI), δ^{13}C, and δ^{18}O data reflect wet/dry climate periods caused by variations of the NAO−/NAO+, whereas the log(Ca/K) data indicate summer temperature caused by direct influence of solar activity on Ca precipitation.

Several climate periods were identified. The DACP (AD 450–750) shows relatively cold and dry periods. In the first phase of the MCA (AD 950–1000), the climate was warm and wet. This was then followed by cold and dry climate between AD 1000–1150. Here, the MS (SI) was relatively high, and a sandy lithology was observed, indicating a possible wet period and a contradiction with the other proxies (radiography, MS [SI], δ^{13}C, and δ^{18}O). The increases in MS and sandy lithology are due to erosion of coarser materials into the lake. The last part of the MCA (AD 1150–1250) was warmer and wetter. In contrast, the LIA (AD 1400–1850) was a period with dry and cold events, as indicated by multiple proxies.

When comparing the Lake Gölcük records with local and regional data, a generally similar climate pattern since ca. AD 400 was observed. However, there were some contradictions due to age uncertainties resulting from the limited ^{14}C dates in those studies. It was noted that all dry/wet periods were associated with NAO+/NAO− and warm/cold periods were associated with an increase/decrease in solar activity. The wet/dry periods were explained by the southward/northward displacement of storm tracks during NAO−/NAO+ conditions. The relationship between warm/cold periods and an increase/decrease in solar activity was explained by the direct influence of solar activity on the lake, leading to an increase in Ca precipitation in the summer.

REFERENCES

Abrantes, F., Rodrigues, T., Rufino, M., Salgueiro, E., Oliveira, D., Gomes, S., Oliveira, P., *et al.*, 2017. The climate of the Common Era off the Iberian Peninsula. *Climate of the Past* **13**, 1901–1918.

Ait Brahim, Y., Khodri, M., Sifeddine, A., Jochum, K.P., Beraaouz, E.H., Wassenburg, J.A., Pérez-Zanón, N., *et al.*, 2017. Speleothem records decadal to multidecadal hydroclimate variations in southwestern Morocco during the last millennium. *Earth and Planetary Science Letters* **476**, 1–10.

Akçer Ön, S., 2017. Küçük Buz Çağı'nda Güneş Etkisine Bağlı İklim Değişimleri: Köyceğiz Gölü Çökel Kayıtları (GB Anadolu) [Climatic variability related to solar activity during the Little Ice Age: Lake Köyceğiz sediment records (SW Anatolia)]. *Türkiye Jeoloji Bülteni* **60**, 569–588. [in Turkish]

Akkemik, Ü., Aras, A., 2005. Reconstruction (1689–1994 AD) of April-August precipitation in the southern part of central Turkey. *International Journal of Climatology* **25**, 537–548.

Andres, H.J., Peltier, W.R., 2016. Regional influences of natural external forcings on the transition from the Medieval climate anomaly to the Little Ice Age. *Journal of Climate* **29**, 5779–5800.

Auger, J.D., Mayewski, P.A., Maasch, K.A., Schuenemann, K.C., Carleton, A.M., Birkel, S.D., Saros, J.E., 2019. 2000 years of North Atlantic-Arctic climate. *Quaternary Science Reviews,* **216**, 1–17.

Baker, A., Hellstrom, J.C., Kelly, B.F.J., Mariethoz, G., Trouet, V., 2015. A composite annual-resolution stalagmite record of North Atlantic climate over the last three millennia. *Scientific Reports* **5**, 10307. https://doi.org/10.1038/srep10307.

Bakker, J., Kaniewski, D., Verstraeten, G., de Laet, V., Waelkens, M., 2012. Numerically derived evidence for late-Holocene climate change and its impact on human presence in the southwest Taurus Mountains, Turkey. *The Holocene* **22**, 425–438.

Bar-Matthews, M., Ayalon, A., Kaufman, A., 1998. Middle to Late Holocene (6,500 yr. period) paleoclimate in the Eastern Mediterranean region from stable isotopic composition of speleothems from Soreq Cave, Israel. In: Issar, A.S., Brown, N. (Eds.), *Water, Environment and Society in Times of Climatic Change. Water Science and Technology Library, Vol. 31.* Springer, Dordrecht, pp. 203–214. https://doi.org/10.1007/978-94-017-3659-6_9

Barlas Şimşek, F., Çağatay, M.N., 2018. Late Holocene high resolution multi-proxy climate and environmental records from Lake Van, eastern Turkey. *Quaternary International* **486**, 57–72.

Blaauw, M., Christen, J. A., 2011. Flexible paleoclimate age-depth models using an autoregressive gamma process. *Bayesian Analysis* **6**, 457–474.

Bookman, R., Enzel, Y., Agnon, A., Stein, M., 2004. Late Holocene lake levels of the dead sea. *Geological Society of America Bulletin* **116**, 555–571.

Bozkurt, D., Sen, O.L., 2011. Precipitation in the Anatolian Peninsula: sensitivity to increased SSTs in the surrounding seas. *Climate Dynamics* **36**, 711–726.

Bozyiğit, C., Eriş, K.K., Sicre, M.A., Çağatay, M.N., Uçarkuş, G., Klein, V., Gasperini, L., 2022. Middle–Late Holocene climate and hydrologic changes in the Gulf of Saros (NE Aegean Sea). *Marine Geology* **443**, 106688. https://doi.org/10.1016/j.margeo.2021.106688.

Brahim, Y.A., Wassenburg, J.A., Cruz, F.W., Sifeddine, A., Scholz, D., Bouchaou, L., Dassié, E.P., Jochum, K.P., Edwards, R.L., Cheng, H., 2018. Multi-decadal to centennial hydro-climate variability and linkage to solar forcing in the Western Mediterranean during the last 1000 years. *Scientific Reports* **8**, 17446. https://doi.org/10.1038/s41598-018-35498-x.

Brázdil, R., Kiss, A., Luterbacher, J., Nash, D.J., Řezníčková, L., 2018. Documentary data and the study of the past droughts: an overview of the state of the art worldwide. *Climate of the Past* **14**, 1915–1960.

Büntgen, U., Myglan, V.S., Ljungqvist, F.C., McCormick, M., Di Cosmo, N., Sigl, M., Jungclaus, J., et al., 2016. Cooling and societal change during the Late Antique Little Ice Age from 536 to around 660 AD. *Nature Geoscience* **9**, 231–236.

Canpolat, E., 2015. Gölcük Volkanik Alanının Jeomorfolojisi, Isparta—Türkiye. *Coğrafya Dergisi* **31**, 62–82. [in Turkish]

Cengiz, O., Sener, E., Yagmurlu, F., 2006. A satellite image approach to the study of lineaments, circular structures and regional geology in the Golcuk Crater district and its environs (Isparta, SW Turkey). *Journal of Asian Earth Sciences* **27**, 155–163.

Cohen, S.A., 2003. *Paleolimnology: The History and Evolution of Lake Systems.* Oxford University Press, Oxford, UK, and New York.

Cook, B.I., Anchukaitis, K.J., Touchan, R., Meko, D.M., Cook, E.R., 2016. Spatiotemporal drought variability in the Mediterranean over the last 900 years. *Journal of Geophysical Research* **121**, 2060–2074.

Corella, J.P., Stefanova, V., El Anjoumi, A., Rico, E., Giralt, S., Moreno, A., Plata-Montero, A., Valero-Garcés, B.L., 2013. A 2500-year multi-proxy reconstruction of climate change and human activities in northern Spain: the Lake Arreo record. *Palaeogeography, Palaeoclimatology, Palaeoecology* **386**, 555–568.

Cronin, T.M., Hayo, K., Thunell, R.C., Dwyer, G.S., Saenger, C., Willard, D.A., 2010. The Medieval Climate Anomaly and Little Ice Age in Chesapeake Bay and the North Atlantic Ocean. *Palaeogeography, Palaeoclimatology, Palaeoecology* **297**, 299–310.

Croudace, I.W., Löwemark, L., Tjallingii, R, Zolitschka, B., 2019. Current perspectives on the capabilities of high resolution XRF core scanners. *Quaternary International* **514**, 5–15.

Croudace, I.W., Rindby, A., Rothwell, R.G., 2006. ITRAX: description and evaluation of a new multi-function X-ray core scanner. *Geological Society, London, Special Publications* **267**, 51–63.

Cullen, H.M., deMenocal, P.B., 2000. North Atlantic influence on Tigris-Euphrates streamflow. *International Journal of Climatology* **20**, 853–863. https://doi.org/10.1002/1097-0088(20000630)20:8<853::AID-JOC497>3.0.CO;2-M.

Danladi, I.B., Akçer-Ön, S., 2018. Solar forcing and climate variability during the past millennium as recorded in a high altitude lake: Lake Salda (SW Anatolia). *Quaternary International,* **486**, 185–198.

Danladi, I.B., Akçer-Ön, S., Ön, Z.B., Schmidt, S., 2021. High-resolution temperature and precipitation variability of southwest Anatolia since 1730 CE from Lake Gölcük sedimentary records. *Turkish Journal of Earth Sciences* **30**. https://doi.org/10.3906/yer-2008-14.

Davies, S.J., Lamb, H.F., Roberts, S.J., 2015. Micro-XRF core scanning in palaeolimnology: recent developments. In: Croudace, I., Rothwell, R. (Eds.), *Micro-XRF Studies of Sediment Cores. Developments in Paleoenvironmental Research, Vol 17.* Springer, Dordrecht, pp. 189–226.

Delaygue, G., Bard, E., 2011. An Antarctic view of Beryllium-10 and solar activity for the past millennium. *Climate Dynamics* **36**, 2201–2218.

Deniz, A., Toros, H., Incecik, S., 2011. Spatial variations of climate indices in Turkey. *International Journal of Climatology* **31**, 394–403.

DSİ (Devlet Su İşleri Genel Müdürlüğü) [General Directorate of State Hydraulic Works], 1978. *Gölcük Gölü Batimetri Haritası [Bathymetry Map of Gölcük Lake].* DSİ, Ankara, Turkey. [in Turkish].

Eddy, J.A., 1976. The Maunder Minimum: the reign of Louis XIV appears to have been a time of real anomaly in the behavior of the sun. *Science* **192**, 1189–1202.

England, A., Eastwood, W.J., Roberts, C.N., Turner, R., Haldon, J.F., 2008. Historical landscape change in Cappadocia (central Turkey): a palaeoecological investigation of annually laminated sediments from Nar Lake. *The Holocene* **18**, 1229–1245.

Engstrom, D.R., Wright, H.E., 1984. Chemical stratigraphy of lake sediments as a record of environmental change. In: Haworth, E.Y., Lund, J.W.G. (Eds.), *Lake Sediments and Environmental History: Studies in Palaeolimnology and Palaeoecology in Honour of Winifred Tutin.* Leicester University Press, Leicester, UK.

Enzel, Y., Bookman, R., Sharon, D., Gvirtzman, H., Dayan, U., Ziv, B., Stein, M., 2003. Late Holocene climates of the Near East deduced from Dead Sea level variations and modern regional winter rainfall. *Quaternary Research* **60**, 263–273.

Erginal, A.E., ÇaĞatay, M.N., Selim, H.H., KarabiyiKoğlu, M., Çakir, Ç., Yakupoğlu, N., Acar, D., Akbaş, A., Kaya, H., 2019. Multi-proxy sedimentary records of dry-wet climate cycles during the last 2 ka from Lake Çildir, east Anatolian Plateau, Turkey. *Geografia Fisica e Dinamica Quaternaria* **42**, 61–70.

Faegri, K., Iversen, J., 1989. *Textbook of Pollen Analysis.* John Wiley and Sons, Chichester, UK.

Filzmoser, P., Hron, K., 2008. Outlier detection for compositional data using robust methods. *Mathematical Geosciences* **40**, 233–248.

Filzmoser, P., Hron, K., Reimann, C., Garrett, R., 2009. Robust factor analysis for compositional data. *Computers & Geosciences* **35**, 1854–1861.

Filzmoser, P., Hron, K., Templ, M., 2018. *Applied Compositional Data Analysis: With Worked Examples in R.* Springer Nature, Cham, Switzerland. https://doi.org/10.1007/978-3-319-96422-5.

Frisia, S., Borsato, A., Spötl, C., Villa, I., Cucchi, F., 2005. Climate variability in the SE Alps of Italy over the past 17 000 years reconstructed from a stalagmite record. *Boreas* **34**, 445–455.

Göktürk, O.M., Fleitmann, D., Badertscher, S., Cheng, H., Edwards, R.L., Leuenberger, M., Fankhauser, A., Tüysüz, O., Kramers, J., 2011.

Climate on the southern Black Sea coast during the Holocene: implications from the Sofular Cave record. *Quaternary Science Reviews* 30, 2433–2445.

Goosse, H., Arzel, O., Luterbacher, J., Mann, M.E., Renssen, H., Riedwyl, N., Timmermann, A., Xoplaki, E., Wanner, H., 2006. The origin of the European "Medieval Warm Period." *Climate of the Past* 2, 99–113.

Grauel, A.L., Goudeau, M.L.S., de Lange, G.J., Bernasconi, S.M., 2013. Climate of the past 2500 years in the Gulf of Taranto, central Mediterranean Sea: a high-resolution climate reconstruction based on $\delta^{18}O$ and $\delta^{13}C$ of *Globigerinoides ruber* (White). *The Holocene* 23, 1440–1446.

Grimm, E.C., 1987. CONISS: a FORTRAN 77 program for stratigraphically constrained cluster analysis by the method of incremental sum of squares. *Computers and Geosciences* 13, 13–35.

Haldon, J., 2016. Cooling and societal change. *Nature Geoscience* 9, 191–192.

Han, D., Gao, C., Yu, Z., Yu, X., Li, Y., Cong, J., Wang, G., 2019. Late Holocene vegetation and climate changes in the Great Hinggan Mountains, northeast China. *Quaternary International* 532, 138–145.

Heinrich, I., Touchan, R., Dorado Liñán, I., Vos, H., Helle, G., 2013. Winter-to-spring temperature dynamics in Turkey derived from tree rings since AD 1125. *Climate Dynamics* 41, 1685–1701.

Helama, S., Jones, P.D., Briffa, K.R., 2017. Dark Ages Cold Period: a literature review and directions for future research. *The Holocene* 27, 1600–1606.

Hernández, A., Sánchez-López, G., Pla-Rabes, S., Comas-Bru, L., Parnell, A., Cahill, N., Geyer, A., Trigo, R.M., Giralt, S., 2020. A 2,000-year Bayesian NAO reconstruction from the Iberian Peninsula. *Scientific Reports* 10, 14961. https://doi.org/10.1038/s41598-020-71372-5.

Jacobson, M.J., Flohr, P., Gascoigne, A., Leng, M.J., Sadekov, A., Cheng, H., Edwards, R.L., Tüysüz, O., Fleitmann, D., 2021. Heterogenous Late Holocene climate in the eastern Mediterranean—the Kocain Cave record from SW Turkey. *Geophysical Research Letters* 48, e2021GL094733. https://doi.org/10.1029/2021GL094733.

Jiang, Y., Xu, Z., 1986. On the Spörer Minimum. *Astrophysics and Space Science* 118, 159–162.

Jones, M.D., Roberts, C.N., Leng, M.J., Türkeş, M., 2006. A high-resolution late Holocene lake isotope record from Turkey and links to North Atlantic and monsoon climate. *Geology* 34, 361–364.

Kahya, E., 2011. The Impacts of NAO on the Hydrology of the Eastern Mediterranean. In: Vicente-Serrano, S., Trigo, R. (Eds.), *Hydrological, Socioeconomic and Ecological Impacts of the North Atlantic Oscillation in the Mediterranean Region. Advances in Global Change Research, Vol 46*. Springer, Dordrecht, pp. 57–71.

Kaniewski, D., Van Campo, E., Paulissen, E., Weiss, H., Bakker, J., Rossignol, I., Van Lerberghe, K., 2011. The Medieval Climate Anomaly and the Little Ice Age in coastal Syria inferred from pollen-derived palaeoclimatic patterns. *Global and Planetary Change* 78, 178–187.

Kılıç, N.K., Caner, H., Erginal, A.E., Ersin, S., Selim, H.H., Kaya, H., 2018. Environmental changes based on multi-proxy analysis of core sediments in Lake Aktaş Turkey: preliminary results. *Quaternary International* 486, 89–97.

Köse, E., 2018. İçel'de Bir Celâlî: Muslu Çavuş İsyani (1606–1610). *Tarih Dergisi* 67, 23–58.

Köse, N., Tuncay Güner, H., Harley, G.L., Guiot, J., 2017. Spring temperature variability over Turkey since 1800 CE reconstructed from a broad network of tree-ring data. *Climate of the Past* 13, 1–15.

Koutsodendris, A., Brauer, A., Reed, J.M., Plessen, B., Friedrich, O., Hennrich, B., Zacharias, I., Pross, J., 2017. Climate variability in SE Europe since 1450 AD based on a varved sediment record from Etoliko Lagoon (western Greece). *Quaternary Science Reviews* 159, 63–76.

Kuhlmann, H., Meggers, H., Freudenthal, T., Wefer, G., 2004. The transition of the monsoonal and the N Atlantic climate system off NW Africa during the Holocene. *Geophysical Research Letters* 31. https://doi.org/10.1029/2004GL021267

Kushnir, Y., Stein, M., 2010. North Atlantic influence on 19th–20th century rainfall in the Dead Sea watershed, teleconnections with the Sahel, and implication for Holocene climate fluctuations. *Quaternary Science Reviews* 29, 3843–3860.

Kushnir, Y., Stein, M., 2019. Medieval climate in the Eastern Mediterranean: instability and evidence of solar forcing. *Atmosphere* 10, 29. https://doi.org/10.3390/atmos10010029.

Kutiel, H., Maheras, P., Türkeş, M., Paz, S., 2002. North Sea–Caspian pattern (NCP)—an upper level atmospheric teleconnection affecting the eastern Mediterranean—implications on the regional climate. *Theoretical and Applied Climatology* 72, 173–192.

Kuzucuoğlu, C., Dörfler, W., Kunesch, S., Goupille, F., 2011. Mid- to Late-Holocene climate change in central Turkey: the Tecer Lake record. *The Holocene* 21, 173–188.

Li, H.C., Ku, T.L., 1997. $\delta^{13}C$–$\delta^{18}O$ covariance as a paleohydrological indicator for closed-basin lakes. *Palaeogeography, Palaeoclimatology, Palaeoecology* 133, 69–80.

Lüning, S., Gałka, M., Danladi, I.B., Adagunodo, T.A., Vahrenholt, F., 2018. Hydroclimate in Africa during the Medieval Climate Anomaly. *Palaeogeography, Palaeoclimatology, Palaeoecology* 495, 309–322.

Lüning, S., Schulte, L., Garcés-Pastor, S., Danladi, I. B., Gałka, M., 2019. The Medieval Climate Anomaly in the Mediterranean region. *Paleoceanography and Paleoclimatology* 34, 1625–1649.

Luterbacher, J., García-Herrera, R., Akcer-On, S., Allan, R., Alvarez-Castro, M. C., Benito, G., Booth, J., et al., 2012. A review of 2000 years of paleoclimatic evidence in the Mediterranean. In: Lionello, P. (Ed.), *The Climate of the Mediterranean Region: From the Past to the Future*. Elsevier, Amsterdam, pp. 87–185.

Mann, M.E., 2013. The Last Millennium. In: Elias, S.A. (Ed.), *Encyclopedia of Quaternary Science: Second Edition*. Elsevier, Amsterdam.

Mann, M.E., 2002. Medieval Climatic Optimum. In: MacCracken, M.C., Perry, J.S. (Eds.), *Encyclopedia of Global Environmental Change: Volume 1, The Earth System: Physical and Chemical Dimensions of Global Environmental Change*. John Wiley & Sons, Chichester, UK, pp. 514–516.

Mann, M.E., Zhihua, Z., Scott, R., Bradley, R.S., Hughes, M.K., Shindell, D., Ammann, C., Faluvegi, G., Ni, F., 2009. Global signatures and dynamical origins of the Little Ice Age and Medieval Climate Anomaly. *Science* 326, 1256–1260.

Martin-Puertas, C., Tjallingii, R., Bloemsma, M., Brauer, A., 2017. Varved sediment responses to early Holocene climate and environmental changes in Lake Meerfelder Maar (Germany) obtained from multivariate analyses of micro X-ray fluorescence core scanning data. *Journal of Quaternary Science* 32, 427–436.

Maxbauer, D.P., Shapley, M.D., Geiss, C.E., Ito, E., 2019. Holocene climate recorded by magnetic properties of lake sediments in the Northern Rocky Mountains, USA. *The Holocene* 30, 479–484.

Moreno, J., Fatela, F., Leorri, E., Gonçalves, M.A., Gómez-Navarro, J.J., Araújo, M.F., Freitas, M.C., Trigo, R.M., Blake, W.H., Moreno, F., 2019. Foraminiferal evidence of major environmental changes driven by the sun-climate coupling in the western Portuguese coast (14th century to present). *Estuarine, Coastal and Shelf Science* 218, 106–118.

Musk, L.F., 1980. Book reviews: "Oliver, J. E. 1978: Climate and Man's Environment. An Introduction to Applied Climatology. Chichester: John Wiley. vii + 517 pp." *Progress in Physical Geography: Earth and Environment* 4, 299–301.

Ocakoğlu, F., Dönmez, E.O., Akbulut, A., Tunoğlu, C., Kır, O., Açıkalın, S., Erayık, C., Yılmaz, İ.Ö., Leroy, S.A.G., 2016. A 2800-year multi-proxy sedimentary record of climate change from Lake Çubuk (Göynük, Bolu, NW Anatolia). *The Holocene* 26, 205–221.

Platevoet, B., Scaillet, S., Guillou, H., Blamart, D., Nomade, S., Massault, M., Poisson, A., et al., 2008. Pleistocene eruptive chronology of the Gölcük Volcano, Isparta Angle, Turkey. *Quaternaire* 19, 147–156.

Pyrina, M., Moreno-Chamarro, E., Wagner, S., Zorita, E., 2019. Spatial signature of solar forcing over the North Atlantic summer climate in the past millennium. *Earth System Dynamics, Discussions* [Preprint: "this preprint was under review for the journal ESD but the revision was not accepted"]. https://doi.org/10.5194/esd-2019-50.

R Core Team, 2021. *R: A Language and Environment for Statistical Computing*. R Foundation for Statistical Computing, Vienna, Austria. https://www.R-project.org/.

Reimann, C., Filzmoser, P., Garrett, R.G., Dutter, R., 2008. *Statistical Data Analysis Explained. Applied Environmental Statistics with R*. John Wiley and Sons, Chichester, UK.

Reimer, P.J., Bard, E., Bayliss, A., Beck, J.W., Blackwell, P.G., Ramsey, C.B., Buck, C.E., et al., 2013. IntCal13 and Marine13 Radiocarbon

Age Calibration Curves 0–50,000 Years cal BP. *Radiocarbon* **55**, 1869–1887.

Roberts, N., Jones, M.D., Benkaddour, A., Eastwood, W.J., Filippi, M.L., Frogley, M.R., Lamb, H.F., *et al*., 2008. Stable isotope records of late Quaternary climate and hydrology from Mediterranean lakes: the ISOMED synthesis. *Quaternary Science Reviews* **27**, 2426–2441.

Roberts, N., Moreno, A., Valero-Garcés, B.L., Corella, J.P., Jones, M., Allcock, S., Woodbridge, J., *et al*., 2012. Palaeolimnological evidence for an east–west climate see-saw in the Mediterranean since AD 900. *Global and Planetary Change* **84–85**, 23–34.

Sachs, J.P., Sachse, D., Smittenberg, R.H., Zhang, Z., Battisti, D.S., Golubic, S., 2009. Southward movement of the Pacific Intertropical Convergence Zone AD 1400–1850. *Nature Geoscience* **2**, 519–525.

Schilman, B., Ayalon, A., Bar-Matthews, M., Kagan, E.J., Almogi-Labin, A., 2002. Sea-land paleoclimate correlation in the Eastern Mediterranean region during the Late Holocene. *Israel Journal of Earth Sciences* **51**, 181–190.

Schmitt, A.K., Danišík, M., Siebel, W., Elitok, Ö., Chang, Y.W., Shen, C.C., 2014. Late Pleistocene zircon ages for intracaldera domes at Gölcük (Isparta, Turkey). *Journal of Volcanology and Geothermal Research* **286**, 24–29.

Seguin, J., Bintliff, J.L., Grootes, P.M., Bauersachs, T., Dörfler, W., Heymann, C., Manning, S.W., *et al*., 2019. 2500 years of anthropogenic and climatic landscape transformation in the Stymphalia polje, Greece. *Quaternary Science Reviews* **213**, 133–154.

Şenkul, Ç., Memiş, T., Eastwood, W.J., Doğan, U., 2018. Mid-to Late-Holocene paleovegetation change in vicinity of Lake Tuzla (Kayseri), Central Anatolia, Turkey. *Quaternary International* **486**, 98–106.

Stockmarr, J., 1971. Tablets with spores used in absolute pollen analysis. *Pollen et Spores* **13**, 615–621.

Swingedouw, D., Terray, L., Cassou, C., Voldoire, A., Salas-Mélia, D., Servonnat, J., 2011. Natural forcing of climate during the last millennium: fingerprint of solar variability. *Climate Dynamics* **36**, 1349–1364.

Thiéblemont, R., Matthes, K., Omrani, N.E., Kodera, K., Hansen, F., 2015. Solar forcing synchronizes decadal North Atlantic climate variability. *Nature Communications* **6**, 8268. https://doi.org/10.1038/ncomms9268.

Thompson, R., Battarbee, R.W., O'Sullivan, P.E., Oldfield, F., 1976. Magnetic susceptibility of lake sediments. *Limnology and Oceanography* **20**, 687–698.

Touchan, R., Akkemik, Ü., Hughes, M.K., Erkan, N., 2007. May–June precipitation reconstruction of southwestern Anatolia, Turkey during the last 900 years from tree rings. *Quaternary Research* **68**, 196–202.

Touchan, R., Xoplaki, E., Funkhouser, G., Luterbacher, J., Hughes, M.K., Erkan, N., Akkemik, Ü., Stephan, J., 2005. Reconstructions of spring/summer precipitation for the Eastern Mediterranean from tree-ring widths and its connection to large-scale atmospheric circulation. *Climate Dynamics* **25**, 75–98.

Tudryn, A., Tucholka, P., Özgûr, N., Gibert, E., Elitok, O., Kamaci, Z., Massault, M., Poisson, A., Platevoet, B., 2013. A 2300-year record of

environmental change from SW Anatolia, Lake Burdur, Turkey. *Journal of Paleolimnology* **49**, 647–662.

Turner, G.M., 1997. Environmental magnetism and magnetic correlation of high resolution lake sediment records from Northern Hawke's Bay, New Zealand. *New Zealand Journal of Geology and Geophysics* **40**, 287–298.

Viana, J.C.C., Sifeddine, A., Turcq, B., Albuquerque, A.L.S., Moreira, L.S., Gomes, D.F., Cordeiro, R.C., 2014. A late Holocene paleoclimate reconstruction from Boqueirão Lake sediments, northeastern Brazil. *Palaeogeography, Palaeoclimatology, Palaeoecology* **415**, 117–126.

Wagner, S., Zorita, E., 2005. The influence of volcanic, solar and CO_2 forcing on the temperatures in the Dalton Minimum (1790–1830): a model study. *Climate Dynamics* **25**, 205–218.

Weber, M.E., Niessen, F., Kuhn, G., Wiedicke, M., 1996. Calibration and application of marine sedimentary physical properties using a multi-sensor core logger. *Marine Geology* **136**, 151–172.

Weltje, G., Tjallingii, R., 2008. Calibration of XRF core scanners for quantitative geochemical logging of sediment cores: theory and application. *Earth and Planetary Science Letters* **274**, 423–438.

White, S., 2012. The Celali Rebellion. In: White, S., *The Climate of Rebellion in the Early Modern Ottoman Empire*. Cambridge University Press, Cambridge, UK, pp. 163–186.

White, S., 2013. The Little Ice Age crisis of the Ottoman Empire: a conjuncture in Middle East environmental history. In: Mikhail, A. (Ed.), *Water on Sand: Environmental Histories of the Middle East and North Africa*. Oxford University Press, Oxford, UK and New York, pp. 71–90.

Wick, L., Lemcke, G., Sturm, M., 2003. Evidence of Late glacial and Holocene climatic change and human impact in eastern Anatolia: high-resolution pollen, charcoal, isotopic and geochemical records from the laminated sediments of Lake Van, Turkey. *The Holocene* **13**, 665–675.

Woodbridge, J., Roberts, N., 2011. Late Holocene climate of the Eastern Mediterranean inferred from diatom analysis of annually-laminated lake sediments. *Quaternary Science Reviews* **30**, 3381–3392.

Xoplaki, E., Fleitmann, D., Luterbacher, J., Wagner, S., Haldon, J. F., Zorita, E., Telelis, I., Toreti, A., Izdebski, A., 2016. The Medieval Climate Anomaly and Byzantium: a review of the evidence on climatic fluctuations, economic performance, and societal change. *Quaternary Science Reviews* **136**, 229–252.

Yukimoto, S., Kodera, K., Thiéblemont, R., 2017. Delayed North Atlantic response to solar forcing of the stratospheric polar vortex. *Scientific Online Letters on the Atmosphere* (*SOLA*) **13**, 53–58.

Żarczyński, M., Wacnik, A., Tylmann, W., 2019. Tracing lake mixing and oxygenation regime using the Fe/Mn ratio in varved sediments: 2000 year-long record of human-induced changes from Lake Żabińskie (NE Poland). *Science of the Total Environment* **657**, 585–596.

Zeist, W. van, Woldring, H., Stapert, D., 1975. Late Quaternary vegetation and climate of southwestern Turkey. *Palaeohistoria* **17**, 53–143. https://ugp.rug.nl/Palaeohistoria/article/view/24805.